External surface cracked offshore steel pipes reinforced with composite repair system subjected to cyclic bending

An experimental investigation

Li, Zongchen; Jiang, Xiaoli; Hopman, Hans; Zhu, Ling; Liu, Zhiping

DOI
10.1016/j.tafmec.2020.102703

Publication date
2020

Document Version
Final published version

Published in
Theoretical and Applied Fracture Mechanics

Citation (APA)
Li, Z., Jiang, X., Hopman, H., Zhu, L., & Liu, Z. (2020). External surface cracked offshore steel pipes reinforced with composite repair system subjected to cyclic bending: An experimental investigation. *Theoretical and Applied Fracture Mechanics*, *109*, Article 102703. https://doi.org/10.1016/j.tafmec.2020.102703

Theoretical and Applied Fracture Mechanics 109 (2020) 102703

Contents lists available at ScienceDirect

Theoretical and Applied Fracture Mechanics

journal homepage: www.elsevier.com/locate/tafmec

External surface cracked offshore steel pipes reinforced with composite repair system subjected to cyclic bending: An experimental investigation

Zongchen Li[a,*], Xiaoli Jiang[a], Hans Hopman[a], Ling Zhu[b], Zhiping Liu[c]

[a] Department of Maritime and Transport Technology, Delft University of Technology, 2628 CD Delft, the Netherlands
[b] Departments of Naval Architecture, Ocean and Structural Engineering, School of Transportation, Wuhan University of Technology, 430063 Wuhan, PR China
[c] Port Logistic Technology and Equipment Research Centre of Ministry of Education, 430063 Wuhan, PR China

ARTICLE INFO

Keywords:
Composite repair system
Offshore steel pipes
External surface crack
Experimental investigation
Fatigue crack growth rate
Structural integrity

ABSTRACT

In this paper, we experimentally studied the external surface crack growth in steel pipes reinforced with Composite System Repaired (CRS). CRS reinforced surface cracked *API 5L X65* pipes were tested, containing three initial notch sizes and four reinforcement schemes. During the tests, the crack growth results, as well as the strain on the external mid-bottom composite laminate around the cracked area, and the vertical deflection of the specimens were recorded. The results showed that within the surface crack growth stage, the composite laminates were adequately bonded on the steel substrate, which significantly decreased the crack growth rate and prolonged the residual fatigue life. In addition, CRS reinforcement has increased the stiffness of the surface cracked pipes. Through the analysis on applying different reinforcement schemes, we indicated that increasing the amount of composite layers evidently facilitated the reinforcement effectiveness, while increasing the bond length did not; and the inversely diagonal wrapping pattern performance less effective.

1. Introduction

Metallic pipes play an irreplaceable role in the offshore industry, acting as the primary way of fluid transportation. They have been widely applied owing to the advantages of cost-effectiveness, simplicity, ease of installation and maintenance. However, metallic pipes are prone to fatigue problems [1]. In marine environment, they bear dynamic loads long-termly. For instance, cyclic bending loads generated by wave, current, wind, and 2nd order floater motions are applied on critical zones. In such situation, surface cracks frequently initiate from surface defects such as corrosion pitting, girth weld defects, or mechanical dents [2,3]. Thereafter, they might continually propagate to through-thickness cracks, eventually resulting in leakage or collapse [4].

Surface cracks need to be repaired instantly to maintain the structural integrity of the pipeline systems towards their design service lives. The Composite Repair System (CRS) has been recognized as an efficient and advanced repairing technique in the piping industry [5]. It has been highly valued for the outstanding advantages in terms of effectiveness, time-saving, cost-effectiveness, no secondary damage and ease of installation [6,7]. At present, CRS on repairing cracked pipes are designed under the guidance of ISO 24,817 [8] and ASME PCC-2 [9], which are based on the ultimate strength theory or the rule of thumb. Their design philosophy aims to rehabilitate the load bearing capacity rather than focusing on the fatigue crack growth rate (FCGR). In recent years, researchers conducted studies on composite repaired fatigue cracked metallic pipes, for the purposes of identifying the repairing mechanism and its effect on the FCGR [10–14]. Failure modes such as crack-induced debonding and their negative effect have been determined as well [15,16]. Those investigations raised the confidence toward the CRS application on repairing the cracked metallic pipes.

To date, the controversy on whether CRS is appropriate for repairing leaking—through-the-thickness cracked pipes, still exists. The rebuttal is that leakage with high pressure will seriously damage the composite laminates. In addition, even under low pressure conditions, the leaked oil and gas might cause considerable erosion to the CRS. As a consequence, cracked metallic pipes should be repaired within the surface cracking stage, in order to prevent leakage and even collapse.

Surface cracks, however, in most cases propagating as a semi-elliptical shape, is more complex than through-thickness cracks in terms of the three-dimensional configuration. They propagate along multiple directions perpendicular to the semi-elliptical crack front, particularly along the depth direction and the length direction. In recent years, relevant studies of using CRS on repairing the surface cracked metallic pipes have been conducted by means of finite element approaches [17,18]. These studies focused on the internal surface cracks, meaning

* Corresponding author.
E-mail address: z.li-8@tudelft.nl (Z. Li).

https://doi.org/10.1016/j.tafmec.2020.102703
Received 19 May 2020; Received in revised form 16 June 2020; Accepted 14 July 2020
Available online 17 July 2020

the composite laminates did not directly contact with the cracked area. Thus the reinforcement effectiveness on decreasing the FCGR was because of the decreasing of the stress value around the cracked area [18]. However, when reinforcing the external surface cracks in metallic pipes, the adhesive layer will directly contact with the cracked area. The direct integration between the CRS and the surface crack can be significant [19,20]. In addition, surface crack growth might trigger interfacial failures in return.

To the knowledge of the authors, the investigation of CRS reinforcement on external surface cracked metallic pipes is absent from open documents. As one of the most reliable methods to understand the reinforcement mechanism and identify the failure modes, the experimental investigation plays an irreplaceable role. Given that, in this paper, we conduct an experimental study on external surface cracked steel pipes reinforced with the CRS subject to cyclic bending. The main purpose is to identify the mechanism of CRS reinforcement on the crack growth. To achieve this, nine groups of 27 specimens in terms of different crack notch sizes, and different reinforcement schemes were tested. In Section 2 the specimen preparation processes are introduced. In Section 3, the test set-up is described. In Section 4, the test phenomenon and results are presented and analysed. Finally the conclusions are drawn in Section 5.

2. Specimen preparation

Specimen preparation is an important step for the sake of achieving ideal experimental results. The quality of each constituent part is needed to be guaranteed. In this section, the preparation procedures including material properties, specimens manufacturing, and specimens configurations are introduced successively.

2.1. Material properties

The sketch diagram of the CRS reinforced external surface cracked steel pipe specimen is shown in Fig. 1. Four materials were used to manufacture the specimens: steel substrate, Glass-FRP (GFRP), Carbon-FRP (CFRP), and adhesive. Stainless steel *API 5L X65* for subsea scenarios conforming to API SPEC 5L code [21] has been used as the steel substrate, which has a yield strength of 448 MPa, and a tensile strength of 530 MPa. In light of the galvanic corrosion between the CFRP laminates and the steel substrate, one layer of GFRP laminate was adopted as the contact inhibitor between the steel substrate and CFRP laminates. The GFRP laminate applied the E-glass fibre weave fabric while the CFRP laminate used the Toray T700S series unidirectional fabric. The adhesive adopted the ZHONGBO ER4080 resin epoxy. The detailed material properties are listed in Tables 1 to 3. Note that all material properties are provided by each manufacturer.

Table 1
Material properties of GFRP.

E_1 (Pa)	E_2 (Pa)	T (Pa)	G_{13} (Pa)	G_{23} (Pa)	Nu
45×10^9	45×10^9	1.1×10^9	4.7×10^9	3.5×10^9	0.33

Note: E_i and G_{ij} are the elastic modulus and shear modulus towards different directions. T is the tensile strength. Nu is the Passion's ratio.

Table 2
Material properties of the CFRP material.

E_1 (Pa)	E_2 (Pa)	T (Pa)	G_{13} (Pa)	G_{23} (Pa)	Nu
230×10^9	25×10^9	4.9×10^9	5.5×10^9	3.9×10^9	0.3

Table 3
Material properties of the resin epoxy.

E (Pa)	T (Pa)	G (Pa)	Nu
2.80×10^9	70×10^6	1.4×10^9	0.35

2.2. Specimen manufacturing

The specimen manufacturing contains three main steps: manufacturing notches, pre-cracking, and the CRS reinforcement, as indicated in Fig. 2. Semi-elliptical notches located in the mid-bottom of the steel pipes were manufactured, as indicated in Fig. 1. They were made by the ASTM E2899 suggested Micro-Electric Discharging Machining (Micro-EDM) method in order to achieve the user designed notch profile and to avoid the thermal residual stress [22]. The aimed aspect ratio of the notches are 0.5, 0.625, and 1.0, representing the range of common seen shapes of surface cracks in offshore metallic pipes in practice [3]. The width and half-length of all notches are controlled as 0.35 mm and 4.0 mm respectively. The shape of the notches guaranteed that the surface cracks would propagate as semi-elliptical shaped during the fatigue tests.

Then, a pre-cracking procedure was conducted on the notched steel pipes, in order to initiate fatigue cracks from the notches [23]. This procedure was conducted on the fatigue machine using the four-point bending (see in Fig. 5), containing two stages: the first stage adopted 80% yield stress of the steel as the amplitude of the sinusoidal cyclic loading, while the second stage adopted 60% yield stress. Note both stages were conducted under the load ratio R equals to 0.1. The pre-cracking procedure continued until the surface crack initiated from the notch and propagated more than 1.0 mm along the length direction, which was monitored by an electronic microscope. Then the size of each surface crack after the pre-cracking procedure was regarded as the initial crack size. The specimens therefore were ready for the CRS

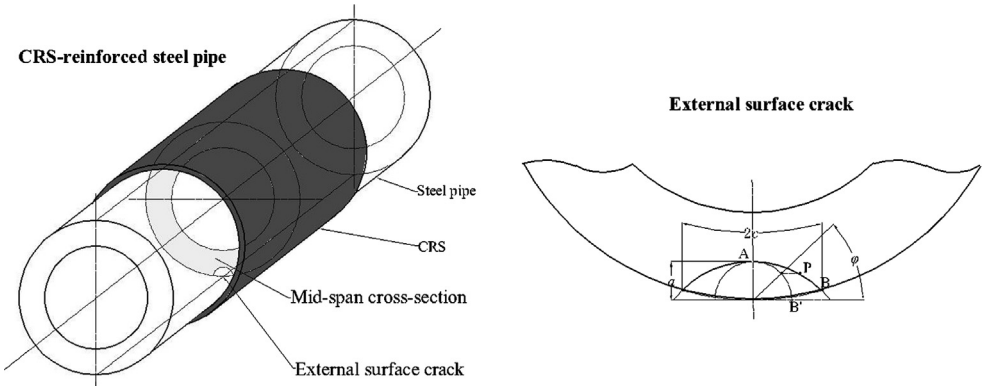

Fig. 1. The sketch diagram of the CRS reinforced surface cracked pipe specimens.

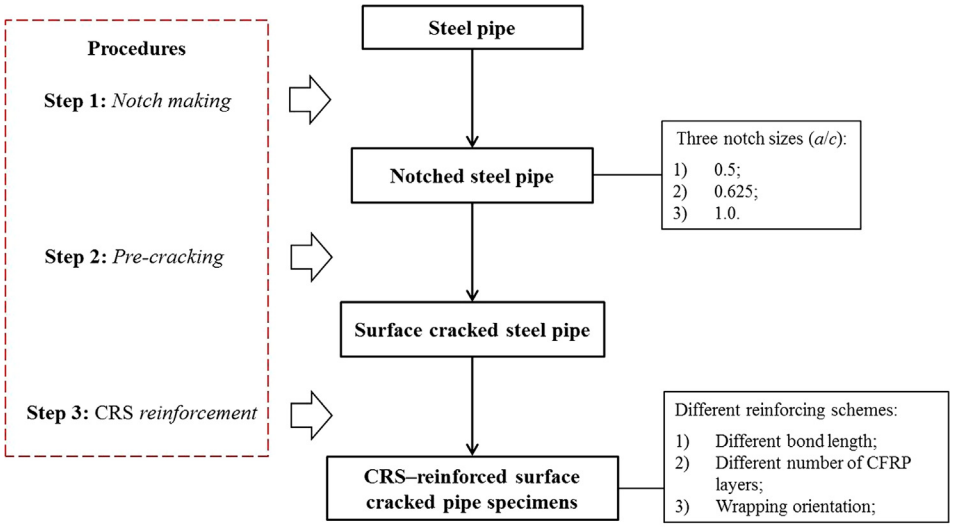

Fig. 2. The procedure of specimen preparation.

reinforcement procedure.

Afterwards, the external surface cracked steel pipes were reinforced with CRS, which was implemented by professional workers using hand lay-up technique. This step contained three procedures: surface preparation, cleaning, and pasting the composite laminates onto the steel substrate. The rust cleaning and sanding process were implemented during the surface preparation procedure. Then the surface of the steel substrate was cleaned using acetone. These implemented surface preparation methods were selected to meet the practical situation to the maximum extent; therefore, more advanced techniques (e.g., abrasive blasting) which might be infeasible in practical situations was not applied. During the pasting procedure, the composite laminates were bonded at the middle of the steel pipes. One layer of GFRP was applied as the first layer for all the CRS reinforced specimens, in order to prevent the galvanic corrosion between the CFRP laminates and the steel substrate. Then the CFRP laminates were wrapped around the cracked pipes using different reinforcement schemes. For instance, different bond lengths, CFRP orientation, number of bond layers. Then the CRS were compressed by wrapping plastic tapes around the external composite layer to squeeze redundant resin epoxy and eliminate the bubbles in the interlaminations. This process guaranteed that the CRS was bonded tightly onto the steel pipe. Finally the reinforced specimens were placed at room temperature for solidification of one week, in order to achieve the optimum bond condition.

2.3. Specimens configurations

The sketch diagram of the CRS reinforced cracked specimen is shown in Fig. 3, and the dimensions of the specimens are listed in Table 4, including the pipe length L, pipe external diameter D, wall thickness of the pipe specimens t, and the depth & half length of the notch a_0 and c_0. The thickness of each layer of GFRP and CFRP laminate are 0.35 mm. In total, nine groups of 27 specimens were prepared. Group 1, 2, 3 are three controlling groups without composite reinforcement. The difference between Groups 1 to 3 is lying in their notch sizes. Groups R1 to R3 are the corresponding groups of Groups 1 to 3 respectively, using the default reinforcement scheme: four layers of CFRP laminates, the 'L-L-L-H' wrapping pattern (L represents longitudinal wrapping pattern, while H represents hoop wrapping pattern) shown in Fig. 4a, and 1,000 mm bond length. The specimens in Groups R4 and R5 applied the same wrapping pattern of Group R1, while using a different bond length L_c and number of bond layers respectively. The difference between Group R6 and Group R1 is that R6 applied the inversely diagonal wrapping method, as indicated in Fig. 4b. Table 4 summarised the configuration and reinforcement details of all specimens. The name of the specimens represents the notch category, CRS reinforcement scheme, CFRP wrapping pattern, and their repetitive number. Take 'PE-1-R(1)' as an example, 'P' means steel pipe, 'E' represents external surface crack, the '1′ stands for the notch category 1, R means reinforcement, and the '(1)' means the No. of the repetitive specimen.

3. Test set-up

The fatigue tests followed the code of ASTM E647 [23]. All tests were carried out under constant amplitude sinusoidal cyclic loading, generated by MTS Hydraulic Actuator, which has a capacity of 1,000 kN. The schematic and the real test set-up are shown in Figs. 5 and 6 respectively. The load was applied in four-point bending condition to ensure a pure bending statue around the cracked location within the inner span. Note that the inner span L_i is designed as 800 mm, which is more than four times larger than the pipe diameter, in order to eliminate potential negative effects from the loading cells. The external span L_e is designed as 1,800 mm, therefore leaving the bending arm equals to 500 mm.

All the fatigue tests were conducted at room temperature and air environment under load control condition. The amplitude of the applied force, namely 241.54 kN, produced a maximum stress value of 268.8 MPa, accounting for 60% of the yield strength of the steel substrate. Such selection is based on the fact the normal stress at the critical zones of a steel lazy-wave riser can reach 240 MPa or even higher [24], as well as considering to adequately reducing the test period. The loading frequency was set as 2.5 Hz. The load ratio R maintained 0.1 for the crack growth process of all tests. The crack growth process was recorded using beach marking technique by means of changing the load ratio R to 0.5 and cycled for 5,000 cycles, as indicated in Fig. 7. Each test ended automatically once the pipe specimen fractured and trigger the displacement limiter of the fatigue machine.

During the fatigue test, the strain on the external CFRP laminate around the middle bottom was monitored. Four strain gauges were installed on each CRS reinforced specimens on the external CFRP laminate along the bottom middle line, as shown in Fig. 8. G1 and G3 were axial symmetry installed by the surface crack along the bottom middle line, so were G2 and G4. The gauges of G3 and G4 were acting as the substitutions for G1 and G2 respectively. The distance between G1 and the middle cross section of the pipe is 30 mm, while G2 was installed adjacent to G1. Then the gauges were connected to the dynamic strain indicator to monitor the strain data for 60 s of every

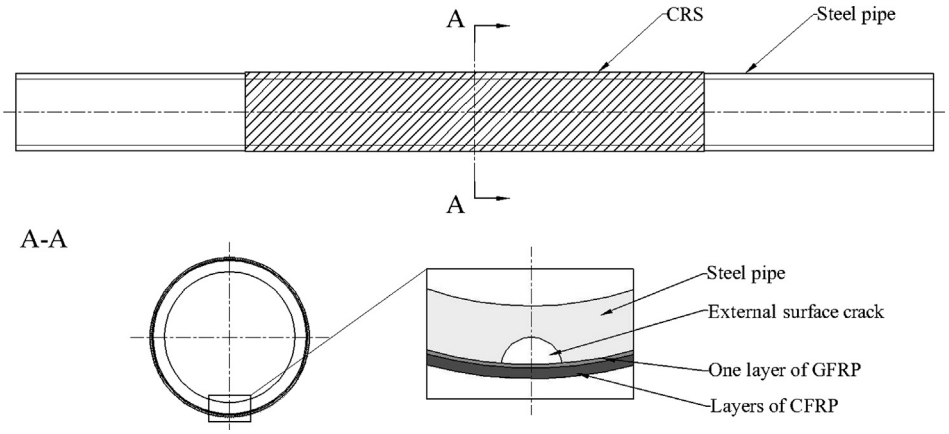

Fig. 3. The configuration of CRS reinforced steep pipe specimens.

10,000 cycles.

Three dial indicators were installed at the bottom side of the specimens as well, each of them was positioned at the one fourth of the external span of the four-point bending (Points B, C and D), connecting to the static indicator, as shown in Fig. 6 and Fig. 9. Point A and E are the points where the steel pipes contacted with the support units, thus their displacement during the test remained zero. During the test, the displacement results of point B, C, and D were recorded for every 10,000 cycles, from 0 kN to the amplitude of the bending load of 241.54 kN.

4. Results and discussion

In this section, the test results, including failure modes, the surface crack growth results, as well as the strain data around the mid-bottom of the specimens and the load–displacement data of the specimens along the bottom middle line, are presented and analysed.

4.1. Failure modes

Within the surface crack growing stage, no failures were observed for all specimens, including interfacial failure, composite delamination, cohesion failures or composite rupture. The CRS was adequately bonded on the steel pipes during the fatigue tests before the crack penetrating the pipe wall. When approaching the end of each test, the crack has already propagated to larger through-thickness cracks, a clearly sound of debonding at the mid-bottom was captured for each CRS reinforced specimen.

4.2. Surface crack growth behaviour and crack growth results

After each test, the cross-sections of bending specimens were sampled around the cracked area by the oxy-acetylene cutting. Then the crack growth behaviour and was recorded by the beach marking technique. Then the crack sizes corresponding to each additional 10,000 cycles under $R = 0.1$ were measured by using an electronic

Table 4
Specimens' configuration and reinforcement details.

Group	Specimen	Notch category	L (mm)	D (mm)	t (mm)	a_0 (mm)	c_0 (mm)	L_c (mm)	CFRP wrapping scheme
1	PE-1(1)	1	2,000	168.3	12.76	2.31	4.94	\	\
	PE-1(2)	1	2,000	168.3	12.81	2.48	5.04	\	\
	PE-1(3)	1	2,000	168.3	12.77	2.44	4.89	\	\
2	PE-2(1)	2	2,000	168.3	12.70	2.39	3.99	\	\
	PE-2(2)	2	2,000	168.3	12.74	2.44	3.82	\	\
	PE-2(3)	2	2,000	168.3	12.68	2.39	3.99	\	\
3	PE-3(1)	3	2,000	168.3	12.61	3.99	4.00	\	\
	PE-3(2)	3	2,000	168.3	12.73	3.96	3.98	\	\
	PE-3(3)	3	2,000	168.3	12.84	3.92	3.97	\	\
R1	PE-1-R(1)	1	2,000	168.3	12.63	2.31	4.94	1,000	L-L-L-H
	PE-1-R(2)	1	2,000	168.3	12.78	2.48	5.035	1,000	L-L-L-H
	PE-1-R(3)	1	2,000	168.3	12.76	2.44	4.885	1,000	L-L-L-H
R2	PE-2-R(1)	2	2,000	168.3	12.71	2.50	3.95	1,000	L-L-L-H
	PE-2-R(2)	2	2,000	168.3	12.68	2.53	3.90	1,000	L-L-L-H
	PE-2-R(3)	2	2,000	168.3	12.78	2.47	4.445	1,000	L-L-L-H
R3	PE-3-R(1)	3	2,000	168.3	12.66	4.03	4.02	1,000	L-L-L-H
	PE-3-R(2)	3	2,000	168.3	12.47	3.95	3.955	1,000	L-L-L-H
	PE-3-R(3)	3	2,000	168.3	12.65	4.02	3.97	1,000	L-L-L-H
R4	PE-1-R600(1)	1	2,000	168.3	12.62	2.47	5.25	600	L-L-L-H
	PE-1-R600(2)	1	2,000	168.3	12.69	2.46	4.92	600	L-L-L-H
	PE-1-R600(3)	1	2,000	168.3	12.74	2.48	4.93	600	L-L-L-H
R5	PE-1-R8(1)	1	2,000	168.3	12.77	2.56	5.09	1,000	L-L-L-H-L-L-L-H
	PE-1-R8(2)	1	2,000	168.3	12.72	2.56	4.90	1,000	L-L-L-H-L-L-L-H
	PE-1-R8(3)	1	2,000	168.3	12.63	2.48	5.15	1,000	L-L-L-H-L-L-L-H
R6	PE-1-R45(1)	1	2,000	168.3	12.74	2.46	4.95	1,000	Inversely diagonal
	PE-1-R45(2)	1	2,000	168.3	12.70	2.50	4.875	1,000	Inversely diagonal
	PE-1-R45(3)	1	2,000	168.3	12.79	2.52	4.87	1,000	Inversely diagonal

Note: The parameters, i.e., D, t, a_0, c_0 were measured based on each specimens, each of which is the weighted average of three measurement locations. The three notch categories represent the three different notch sizes shown in Fig. 2, i.e., aimed aspect ratio of 0.5, 0.625, and 1.0.

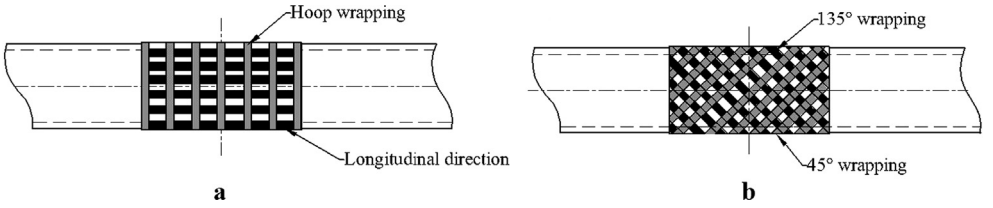

Fig. 4. Wrapping scheme: a) the longitudinal and hoop wrapping pattern; b) the inversely diagonal wrapping pattern.

reading microscope. One random specimen of the repetitive three specimens is selected to show the crack shape variation during the fatigue test, as shown in Fig. 10. The cycle-index between each two adjacent beach marks is 10,000. The figures demonstrate the multiple initiations from the notch fronts, and the surface crack continually propagated as a semi-elliptical shape until the crack penetrated the pipe wall. In addition, the photographs show that the beach marks on the CRS reinforced specimens are denser than on the un-reinforced specimens. Especially, the beach marks of specimens PE-1-R8(2) is significantly denser than PE-1(1), indicating that the FCGR was dramatically reduced by using eight layers of CFRP laminates. The detailed results of crack depth (a) and half crack length (c), corresponding to the cycle-index are listed in the Table A in Appendix.

4.2.1. CRS reinforcement on the cracked steel pipes with different crack size

It is clearly indicated from Figs. 11-13 that the experimental results have a good repeatability. The results of crack growth along the depth direction in Fig. 11a shows that starting from $a = 5.81$ mm (when N is around 25,000 cycles), the CRS prolonged the residual fatigue life from around 65,000 cycles to 110,000 cycles, or approximately 110%. Note that in this paper, the residual fatigue life is defined as the cycle-index from the initiation crack till the crack penetrating the pipe wall. Fig. 11b illustrated that between 30,000 and 60,000 cycles, the cracks barely grew along the length direction. The crack aspect ratio (a/c) variation results in Fig. 11c shows that the a/c of the CRS reinforced specimens were always higher than the non-reinforced specimens. Finally, the preferred aspect ratios (a/c when a/t equals to 0.8) of the CRS reinforced specimens reached around 0.9, which is larger than the unreinforced specimens of 0.8. This indicates that the CRS is more effective on crack growth along the length direction, which might due to the crack-bridging effect.

The results in Figs. 12 and 13 of using CRS to reinforce the specimens with different crack sizes show similar trends with the results in Fig. 11 in terms of the repeatability, fatigue life prolongation, and aspect ratio variation. Fig. 12 indicates that the residual fatigue life has prolonged from 58,000 cycles to 120,000 cycles, of around 110%, and Fig. 13 shows that the residual fatigue life was prolonged around 120%. Besides, the crack of PE-2-R and PE-3-R barely grew along the length direction before the crack length c reached around 7.0 mm. Thus the CRS has a similar effect on surface crack with different crack aspect ratios.

4.2.2. CRS reinforcement on the cracked steel pipes using different bond length

When using composite materials to enhance the strength and stiffness of intact steel pipes, an effective bond length exists: once the bond length has reached a certain value, the effectiveness increases minimal when increasing of the bond length [25]. In this section, crack growth behaviour of the CRS reinforced steel pipes by using different bond length were discussed and analysed. Besides the default length which is 1,000 mm, the less bond length of 600 mm is applied. Fig. 14 illustrates that there is no evident difference of the crack growth between the specimens using the bond lengths of 600 mm and 1,000 mm. This is further illustrated by the $da/dN - \Delta K_a$ and $dc/dN - \Delta K_c$ (see in Fig. 23) that the FCGR along the depth/length direction of PE-1-R and PE-1-R600 are similar. Note that da/dN and dc/dN are the crack growth rate along the depth direction and the length direction respectively. In this sense, there might be an effective bond length for reinforcing the surface cracked steel pipes as well, which could be less than 600 mm.

4.2.3. CRS reinforcement on the cracked surface using different amount of layers

In the previous study, the Stress Intensity Factor (SIF) of internal surface cracked steel pipes reinforced with CRS by using different amount of bond layers has been discussed [18]. The results indicated that the SIF has staged decreased when applying more layers of CFRP [18]. In this section, crack growth behaviour of the CRS reinforced steel pipes by using different amount of bond layers is discussed. Besides the default number of CFRP laminates which is four layers, eight layers is used by doubling the CFRP layers of PE-1-R (see specimens PE-1-R8 in Table 4). Fig. 15a illustrates that the residual fatigue life prolonged dramatically when applying eight layers of CFRP. Starting from 25,000

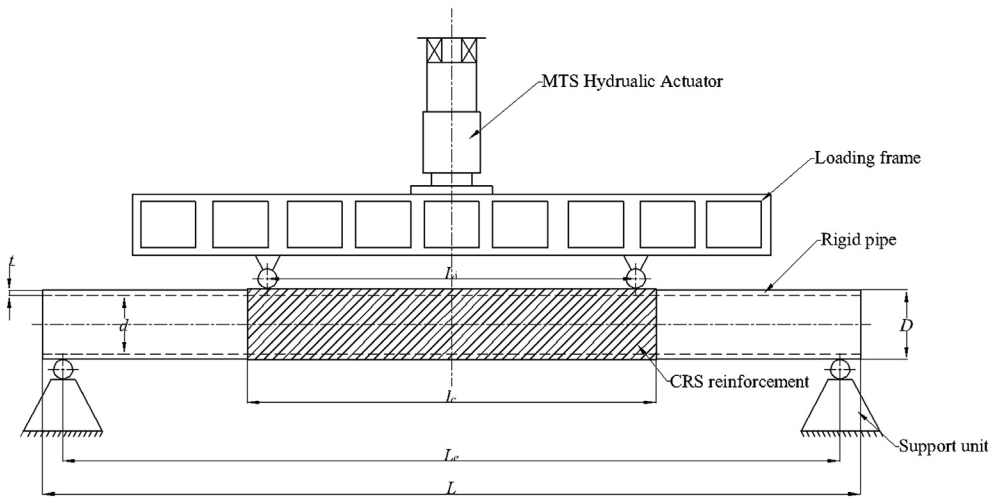

Fig. 5. The schematic of the four-point bending test set-up.

Fig. 6. Specimen and instruments installation.

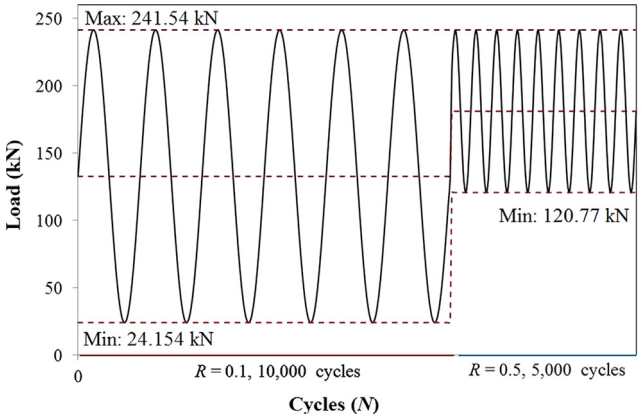

Fig. 7. The load spectrum and beach mark generating procedure.

cycles when a is around 5.8 mm, PE-1-R prolonged the residual fatigue life from 65,000 to 110,000 cycles of 110%, while the PE-1-R8 prolonged the residual fatigue life further to 150,000 cycles, of around 280%. Fig. 15b shows that before the half crack length c reached around 8.0 mm, the increments of crack length of specimens PE-1-R8 are minimal, while the final crack lengths are similar with the specimens of PE-1-R. The aspect ratio variation of PE-1-R8 specimens did not have an evident difference with the PE-1-R specimens, as shown in Fig. 15c.

4.2.4. CRS reinforcement on the cracked surface using different wrapping orientation

In light of the practical situation of applying CRS to repair surface cracked offshore steel pipes – wrapping construction will be taking place under water, the longitudinal wrapping in some cases might be difficult to be implemented. In this sub-section, the default wrapping pattern 'L-L-L-H' is compared with an inversely diagonal wrapping pattern (see in Fig. 4). Fig. 16a and Fig. 16b illustrates that the inversely diagonal wrapping pattern performed less effective than the 'L-L-L-H' wrapping pattern, which prolonged the residual fatigue life of around 66.7%. Fig. 16c shows that there is no evident difference of the aspect ratio variation between the PE-1-R and PE-1-R45 specimens.

4.3. Strain data

Fig. 17 shows the strain data recorded by G1 and G2 gauges for using different schemes to reinforce the first type of crack at the beginning stage (Beg.), middle stage (Mid.) and the last stage (Las.). It is

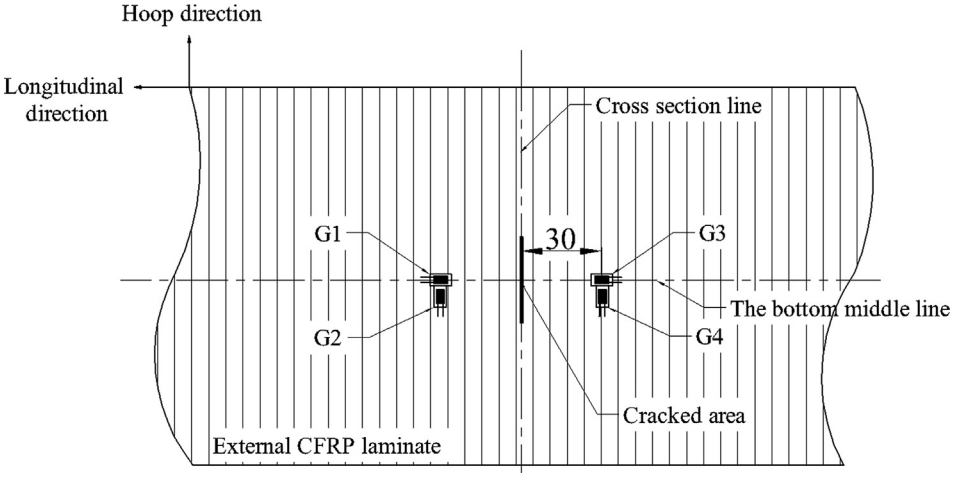

Fig. 8. The installation of strain gauges on the external CFRP laminate around the cracked area.

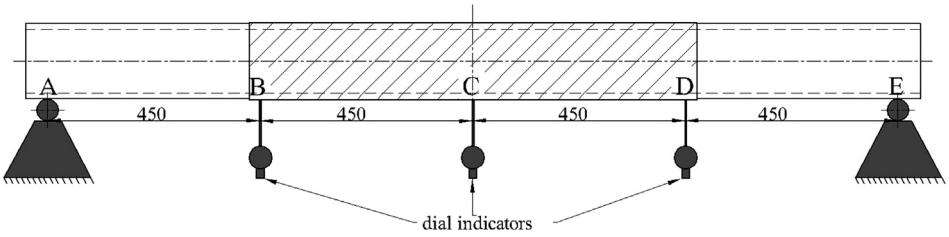

Fig. 9. The dial indicators installed underneath the specimens.

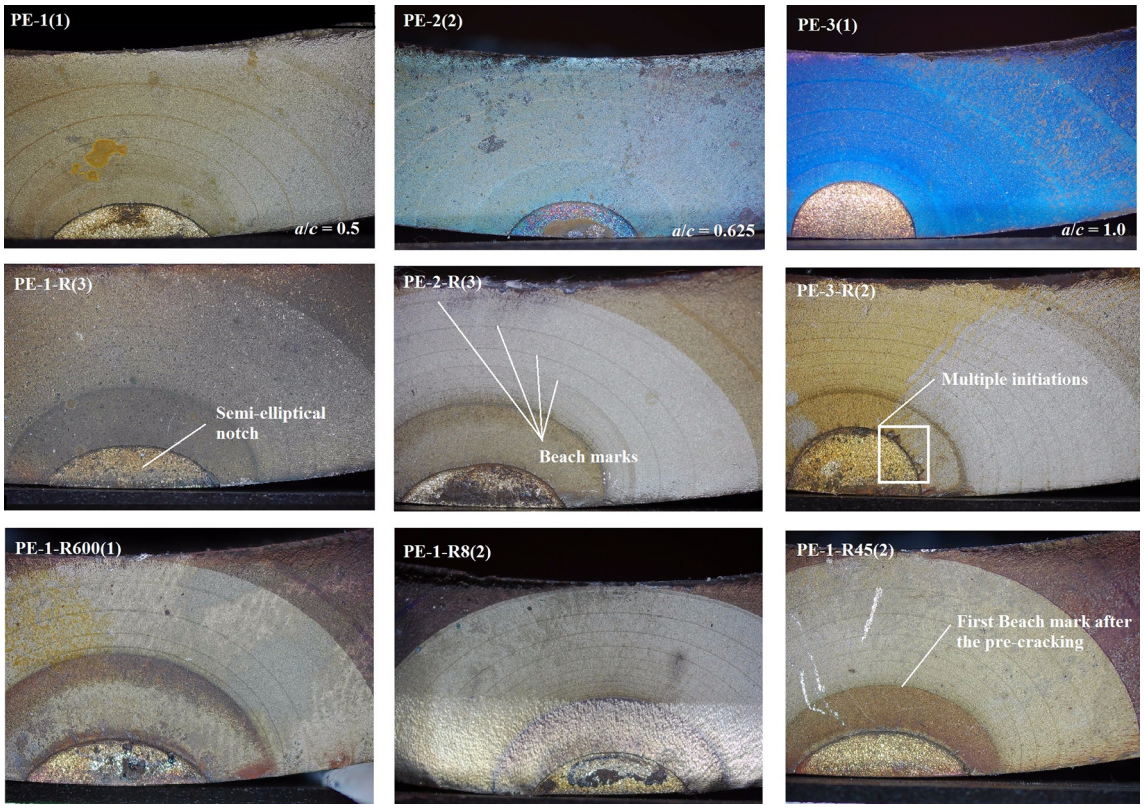

Fig. 10. Beach marks on the cross-section of the steel pipe specimens.

clearly shown that there is no evident difference of the strain results among the beginning, middle, and the last stage for all specimens. The maximum strain value of G1 for PE-1-R(1), PE-1-R8(1) and PE-1-R45(1) are all around 1300 $\mu\varepsilon$, while the maximum strain for PE-1-R45(1) is around 1120 $\mu\varepsilon$, as shown in Fig. 18. The possible reason is that PE-1-R600 has a shorter bond length, the load units therefore contacted with the steel substrate rather than the CFRP laminates (as shown in Fig. 19), thus the stress were transferred from the steel pipes to the CFRP laminates, resulting in smaller strain values. The strain value of PE-1-R8(1) is slightly higher than the PE-1-R(1), owing to the larger external diameter by the doubled layers of CFRP laminates.

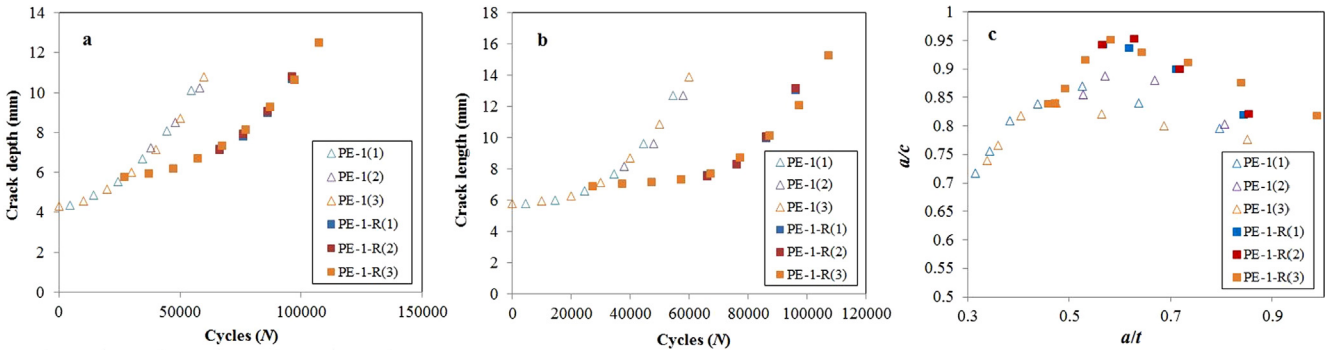

Fig. 11. The experimental results of PE-1 and PE-1-R of using the default reinforcement scheme: a) crack growth along depth direction; b) crack growth along length direction; c) aspect ratio variation: a/c versus a/t curves.

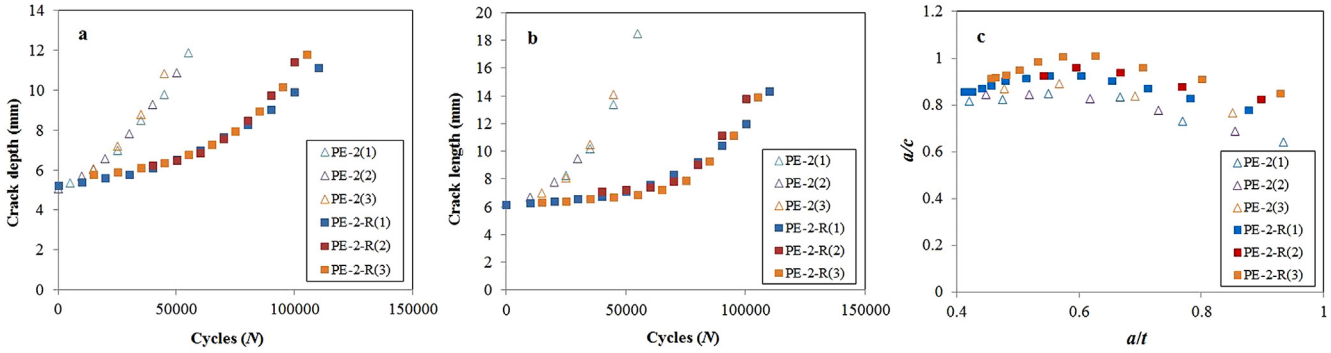

Fig. 12. The experimental results of PE-2 and PE-2-R of using the default reinforcement scheme: a) crack growth along depth direction; b) crack growth along length direction; c) aspect ratio variation: a/c versus a/t curves.

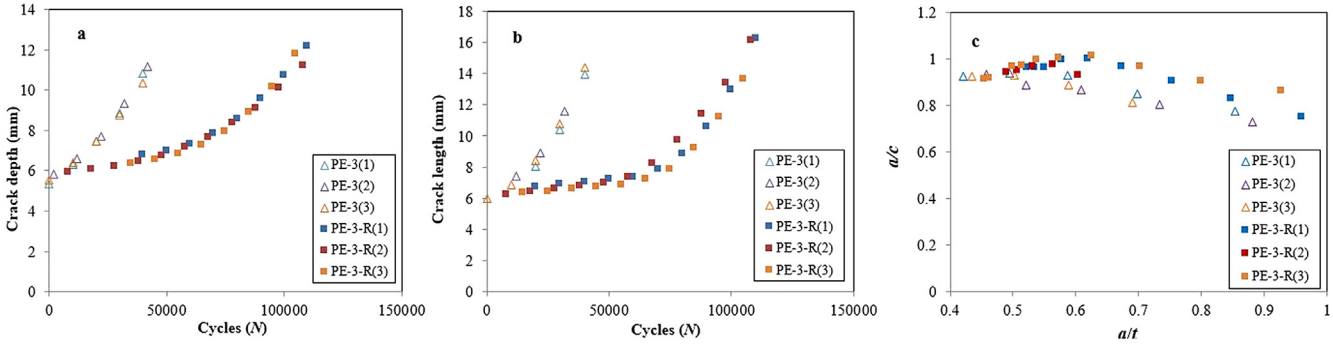

Fig. 13. The experimental results of PE-3 and PE-3-R of using the default reinforcement scheme: a) crack growth along depth direction; b) crack growth along length direction; c) aspect ratio variation: a/c versus a/t curves.

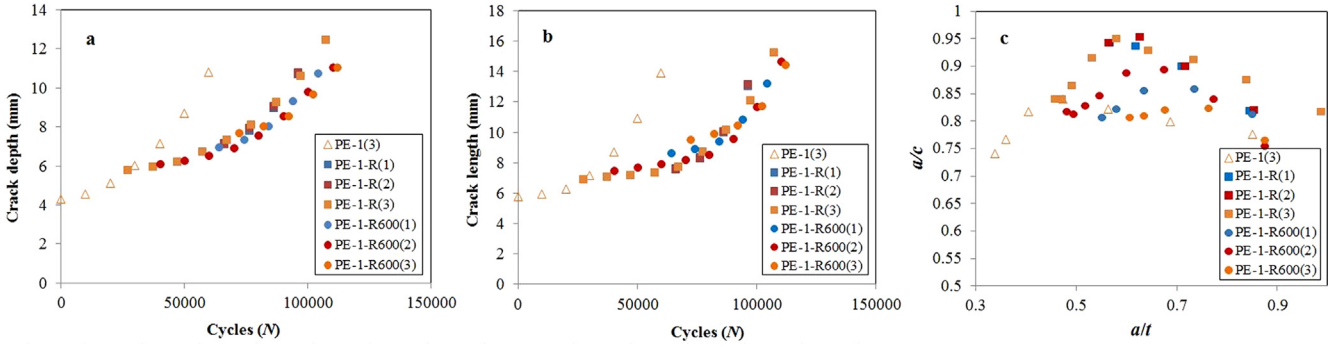

Fig. 14. The experimental result comparison between 1000 mm bond length (PE-1-R) and 600 mm bond length (PE-1-R600) method: a) crack growth along depth direction; b) crack growth along length direction; c) aspect ratio variation: a/c versus a/t curves.

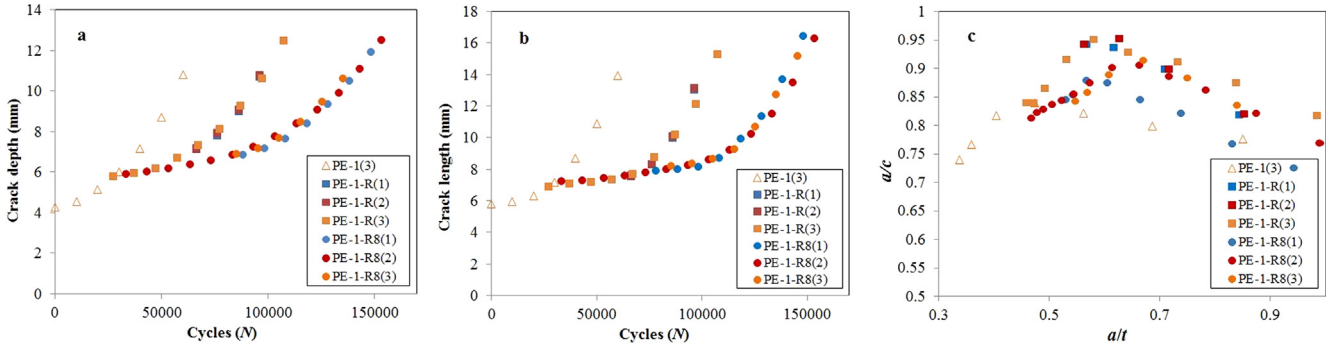

Fig. 15. The experimental result comparison between using four layers of CFRP (PE-1-R) and eight layers of CFRP (PE-1-R8): a) crack growth along depth direction; b) crack growth along length direction; c) aspect ratio variation: a/c versus a/t curves.

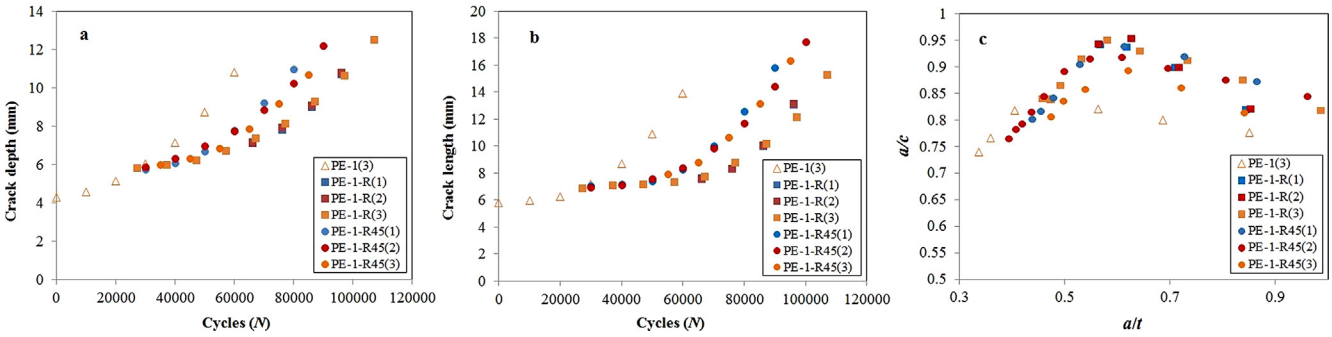

Fig. 16. The experimental result comparison between using L-L-L-H CFRP wrapping (PE-1-R) and inversely diagonal wrapping (PE-1-R45) method: a) crack growth along depth direction; b) crack growth along length direction; c) aspect ratio variation: a/c versus a/t curves.

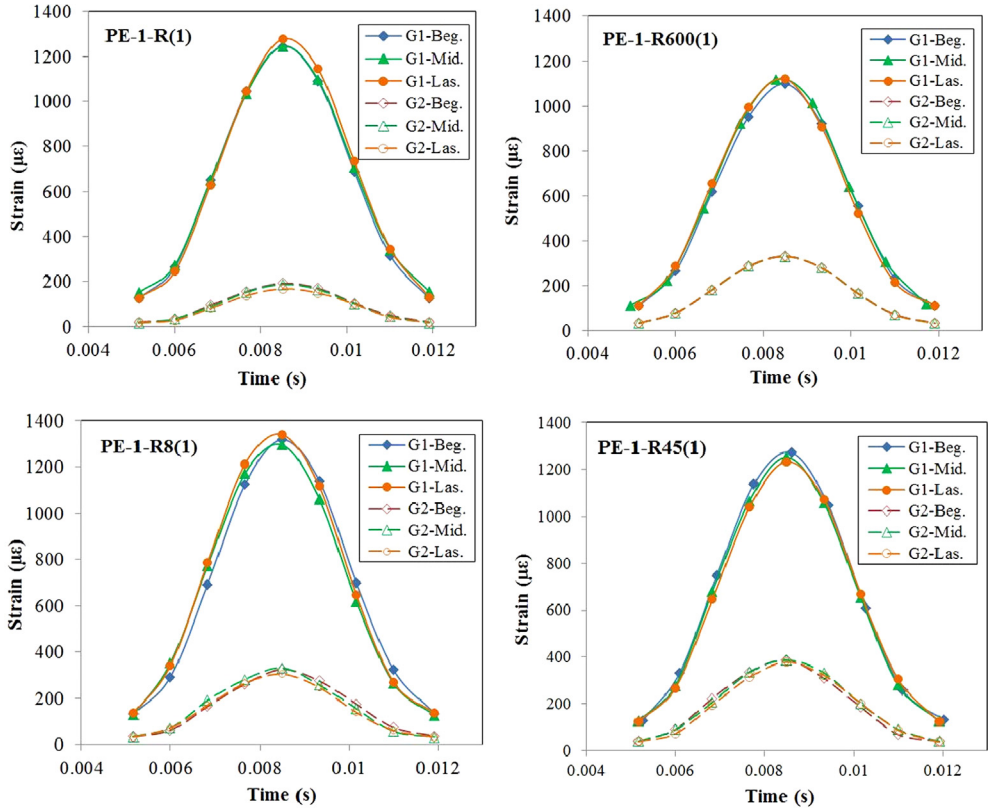

Fig. 17. The strain data of using different scheme to reinforce the type one crack.

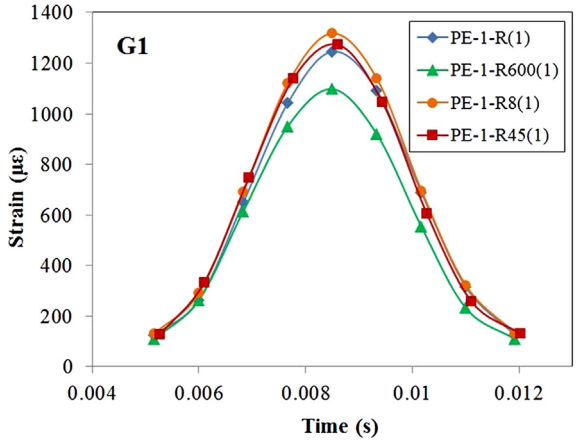

Fig. 18. The strain data at the beginning of each test of using different schemes to reinforce the type one crack.

4.4. Displacement of the specimens

Fig. 20 shows the load–displacement response of the CRS reinforced specimens of using different reinforcement schemes, which clearly illustrates that the displacement response at the beginning stage (Beg.), the middle stage (Mid.), and the last stage (Las.) remained identical. The results indicate that the strength of the CRS reinforced pipes was insensitive to the growth of the surface crack. The comparison of the load–displacement response of different specimens was shown in Fig. 21. The deflection at point C of PE-1-R(1) has decreased by 4.7%, from 3.87 mm to3.69 mm. PE-1-R45(1) has the largest deflection, of 3.82 mm, which is slightly larger than PE-1-R(1) of 3.69 mm and PE-1-R600(1) of 3.72 mm. Specifically, the deflection of PE-1-R8(1), which is 3.36 mm, is dramatically smaller than the rest of the specimens – 13.18% smaller than the unreinforced specimen PE-1(1) and 8.94% smaller than PE-1-R(1). Therefore, increasing the amount of composite layers of CFRP had effectively increased the stiffness of the cracked steel pipe.

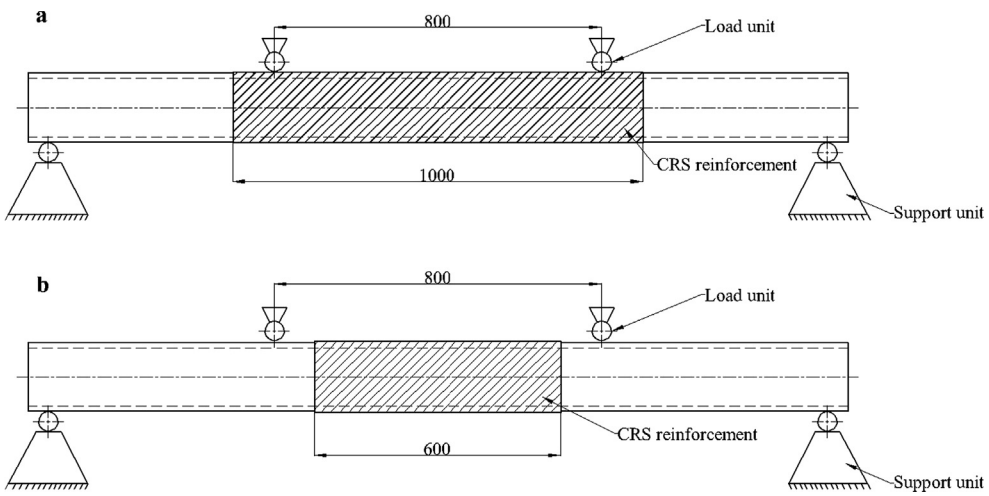

Fig. 19. Loading position of specimens using different bond length: a) PE-1-R and b) PE-1-R600.

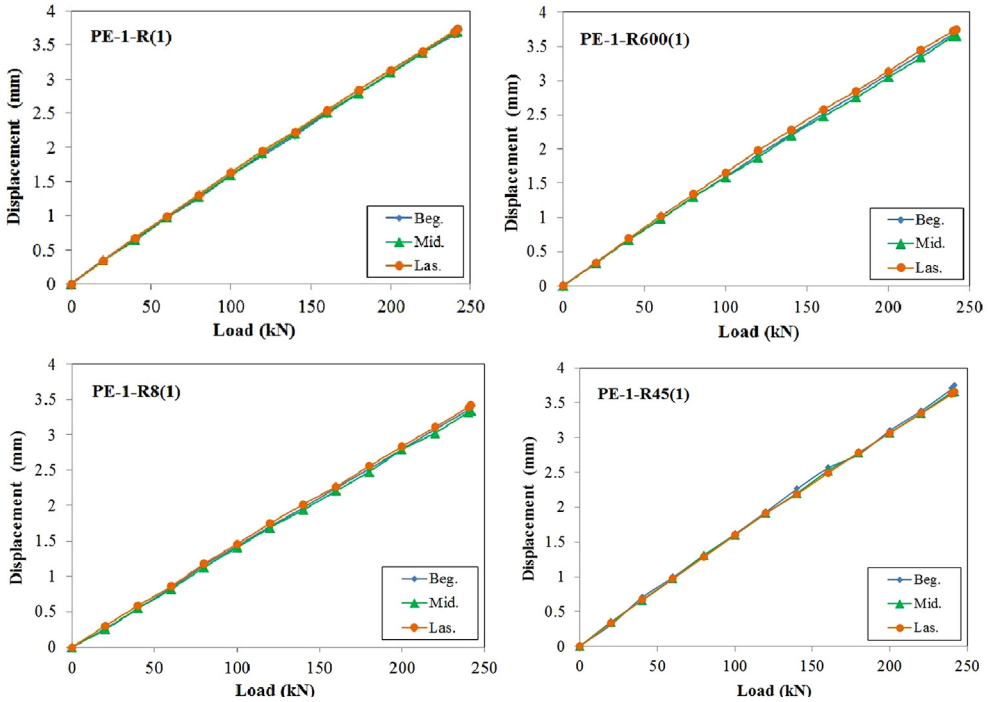

Fig. 20. The displacement data at point C (mid-span displacement) subjected to load from 0 to 241.54 kN.

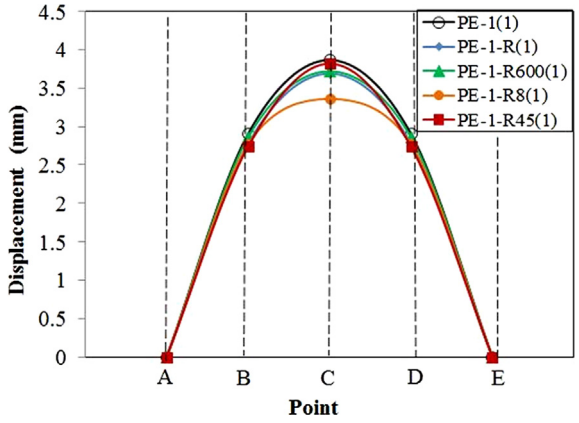

Fig. 21. The displacement data when reaching the amplitude of the fatigue load (241.54 kN).

4.5. Summary of using different reinforcing schemes

In this section, the results in terms of the crack growth, the strain on the external CFRP laminate adjacent to the cracked area, and the load–displacement response are presented and analysed. Fig. 22 summaries the effectiveness of using different reinforcement schemes on the surface crack growth. It shows that there is no evident difference between the specimens of PE-1-R(3) and PE-1-R600(2). Using the inversely diagnose wrapping method is less efficient, while applying eight layers of CFRP laminates preforms the best among the reinforcement methods.

Fig. 23 further displayed the performance of using different reinforcement methods by the $da/dN - \Delta K_a$ and $dc/dN - \Delta K_c$ curves in Fig. 23. Note that ΔK_a and ΔK_c are the range of the SIF of the deepest point and the surface point along the surface crack front respectively, which are calculated by the analytical method proposed in Ref. [2], assuming the surface cracks were not reinforced with CRS. Along the depth direction, PE-1-R(3) and PE-1-R600(2) decreased the FCGR along

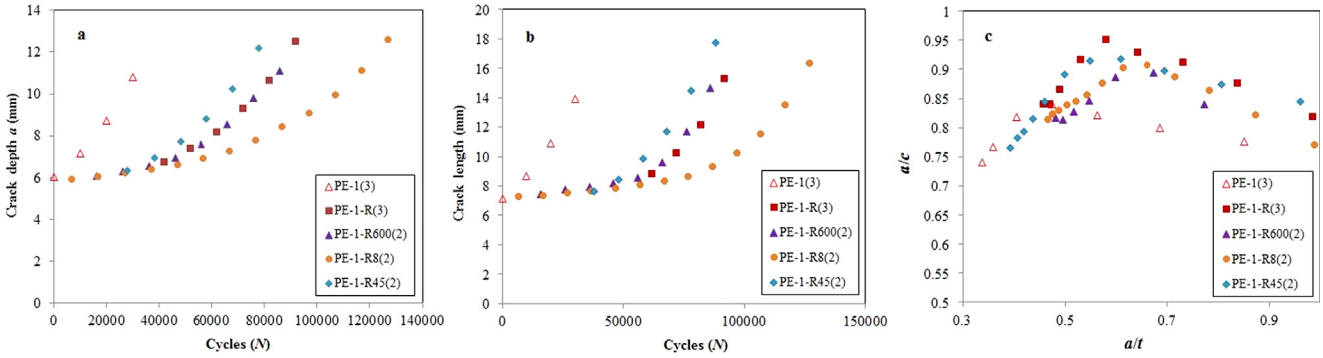

Fig. 22. The experimental result comparison of using different reinforcement schemes.

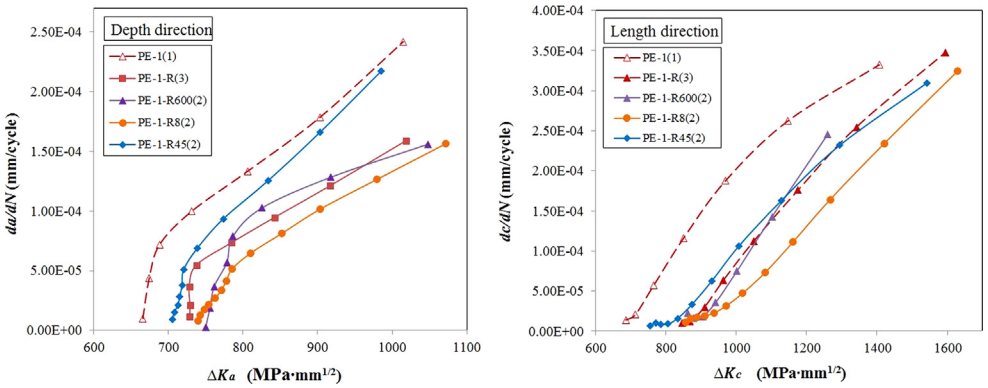

Fig. 23. The experimental result of FCGR comparison of using different reinforcement schemes.

the depth direction approximately 8.3×10^{-5} mm/cycle, while PE-1-R45(2) decreased FCGR around 6.7×10^{-5} mm/cycle, PE-1-R8(2) have significantly reduced the FCGR of 1.22×10^{-4} mm/cycle. The decrease of crack growth along the length is more evident than along the depth direction (see in Fig. 23b), resulting in a shorter crack length when the crack penetrating the pipe wall, illustrated by the larger aspect ratios of the CRS reinforced specimens (see in Fig. 22c).

Through the analysis of the results, we also indicate that the strain and the displacement were insensitive to the surface crack growth. In addition, the load–displacement response of the specimens had a similar pattern with the crack growth reduction response: 1) the specimens of PE-1-R and PE-1-R600 had minimal difference in the crack growth rate, so did the load–displacement response; 2) the specimens of PE-1-R45 had the largest displacement when the load reached the amplitude, the FCGR of PE-1-R45 specimens were the largest as well; 3) the specimens of PE-1-R8 had significantly reduced the FCGR, so did the reinforcement of using eight layers of CFRP on decreasing the vertical deformation.

5. Conclusions

Circumferential external surface crack growth is a serious threat to the structural integrity of offshore steel pipes. Critical surface cracks need to be repaired instantly in order to avoid oil and gas leakage. In this paper, CRS reinforcement on external surface cracked steel pipes subjected to bending has been experimental investigated. In total, nine groups of 27 specimens were tested. The effectiveness of CRS reinforcement on surface cracks with different aspect ratio, different reinforcement schemes in terms of bond length, numbers of bond layer, wrapping orientation has been discussed. The strain data adjacent to the cracked area, load–displacement response, and crack growth results were presented and analysed. The conclusions are drawn:

- The CRS has significantly decreased the FCGR of the surface crack and thus prolonged the residual fatigue life. In this study, under $D/t = 13.25$ and $L_c/L = 0.5$, applying the default reinforcing scheme reduced the FCGR along the depth direction of 8.3×10^{-5} mm/cycle, and prolonged the residual fatigue life of around 110%, while using eight layers of CFRP laminate have maximally decreased the FCGR along the depth direction of 1.22×10^{-4} mm/cycle, thus it prolonged the residual fatigue life of approximately 280%.
- Different from reinforcing internal surface cracks in steel pipes subjected to bending [18], the CRS performed more efficiently on reducing the FCGR along the length direction than along the depth direction, resulting in the increase of the preferred aspect ratio, which might due to the crack-bridging effect.
- The analysis of using different CRS reinforcement schemes indicated that the FCGR of surface cracks is insensitive to the bond lengths applied in this paper, indicating the existence of an effective bond length less than 600 mm; applying more layers of CFRP can significantly promote the reinforcement performance; the inversely wrapping pattern performed less effective than the other wrapping patterns. These analyses have been restricted by the limited number of specimens; further quantitative analysis will be presented in future studies by means of numerical approaches.
- The crack-induced debonding is a serious threat when repairing through-the-thickness cracked metallic structures [16]. While in this study, within the surface crack growth stage, no failures within the composite laminates or within the reinforcement interface were captured. In addition, no evident increase of the FCGR along the length direction was observed. These results indicate that the CRS was adequately bonded on the steel substrate before the surface crack penetrating the pipe wall. Further analysis (e.g., numerical analysis by using cohesive zone modelling) is demanded to reveal its mechanism.
- Integrating with the load–displacement results and the crack growth results, we conclude that the reinforcement effect mainly owed to the decreasing of overall deformation. The crack-bridging effect

Table A1
Surface crack size along the depth and the length direction corresponding to cycle-index (units of *a* and *c* are in mm).

Specimen	PE-1(1)		PE-1(2)		PE-1(3)		PE-2(1)		PE-2(2)		PE-2(3)		PE-3(1)	
Cycles	*a*	*c*	*a*	*c*	*a*	*c*	*a*	*c*	*a*	*c*	*a*	*c*	*a*	*c*
0	3.79	5.51	6.69	7.82	4.29	5.80	5.34	6.53	5.05	6.03	6.07	6.98	5.34	5.78
10,000	3.99	5.56	7.25	8.17	4.57	5.96	6.03	7.33	5.68	6.72	7.2	8.07	6.29	6.71
20,000	4.36	5.77	8.48	9.64	5.14	6.29	6.98	8.24	6.58	7.79	8.79	10.51	7.45	8.01
30,000	4.87	6.02	10.24	12.74	6.02	7.17	8.47	10.16	7.84	9.46	10.81	14.08	8.86	10.43
40,000	5.55	6.62	/	/	7.15	8.71	9.77	13.38	9.27	11.93	/	/	10.84	13.96
50,000	6.67	7.67	/	/	8.720	10.91	11.86	18.46	10.86	15.76	/	/	/	/
60,000	8.09	9.62	/	/	10.80	13.92	/	/	/	/	/	/	/	/
70,000	10.11	12.01	/	/	/	/	/	/	/	/	/	/	/	/

Specimen	PE-3(2)		PE-3(3)		PE-1-R(1)		PE-1-R(2)		PE-1-R(3)		PE-2-R(1)		PE-2-R(2)	
Cycles	*a*	*c*	*a*	*c*	*a*	*c*	*a*	*c*	*a*	*c*	*a*	*c*	*a*	*c*
0	5.82	6.23	5.52	5.96	6.64	7.15	6.47	6.92	5.81	6.92	5.24	6.13	6.24	7.12
10,000	6.61	7.43	6.38	6.86	6.85	7.22	6.72	7.15	5.98	7.12	5.38	6.3	6.49	7.27
20,000	7.72	8.92	7.48	8.43	7.19	7.63	7.15	7.58	6.23	7.20	5.59	6.42	6.87	7.43
30,000	9.32	11.61	8.76	10.77	7.83	8.355	7.95	8.34	6.74	7.36	5.78	6.56	7.55	7.86
40,000	11.18	15.32	10.35	14.4	9.01	10.015	9.09	10.11	7.36	7.74	6.09	6.76	8.48	9.04
50,000	/	/	/	/	10.71	13.075	10.82	13.18	8.16	8.78	6.52	7.13	9.76	11.12
60,000	/	/	/	/	/	/	$> t$	16.89	9.30	10.20	7.00	7.59	11.4	13.82
70,000	/	/	/	/	/	/	/	/	10.64	12.15	7.65	8.3	$> t$	17.16
80,000	/	/	/	/	/	/	/	/	12.51	15.30	8.3	9.21	/	/
90,000	/	/	/	/	/	/	/	/	/	/	9.04	10.4	/	/
100,000	/	/	/	/	/	/	/	/	/	/	9.92	12	/	/
110,000	/	/	/	/	/	/	/	/	/	/	11.14	14.32	/	/

Specimen	PE-2-R(3)		PE-3-R(1)		PE-3-R(2)		PE-3-R(3)		PE-1-R600(1)		PE-1-R600(2)		PE-1-R600(3)	
Cycles	*a*	*c*	*a*	*c*	*a*	*c*	*a*	*c*	*a*	*c*	*a*	*c*	*a*	*c*
0	5.78	6.325	6.53	6.73	5.92	6.235	5.78	6.34	6.99	8.67	6.1	7.465	7.69	9.53
10,000	5.88	6.425	6.64	6.89	6.07	6.425	5.88	6.4	7.35	8.94	6.28	7.725	8.06	9.95
20,000	6.1	6.575	6.79	7.05	6.22	6.605	6.35	6.58	8.06	9.43	6.56	7.925	8.57	10.45
30,000	6.37	6.725	6.98	7.24	6.43	6.78	6.53	6.725	9.33	10.87	6.93	8.185	9.68	11.75
40,000	6.76	6.865	7.33	7.36	6.76	6.985	6.82	6.86	10.78	13.26	7.6	8.565	11.09	14.48
50,000	7.28	7.235	7.86	7.85	7.16	7.345	7.28	7.24	$> t$	16.86	8.56	9.575	$> t$	18.59
60,000	7.95	7.885	8.56	8.87	7.67	8.255	7.95	7.85	/	/	9.81	11.675	/	/
70,000	8.94	9.305	9.56	10.57	8.36	9.695	8.92	9.23	/	/	11.09	14.686	/	/
80,000	10.17	11.165	10.75	12.93	9.1	11.375	10.15	11.21	/	/	/	/	/	/
90,000	11.8	13.895	12.18	16.26	10.09	13.385	11.78	13.65	/	/	/	/	/	/
100,000	$> t$	17.025	/	/	11.2	16.105	$> t$	17.025	/	/	/	/	/	/

Specimen	PE-1-R8(1)		PE-1-R8(2)		PE-1-R8(3)		PE-1-R45(1)		PE-1-R45(2)		PE-1-R45(3)	
Cycles	*a*	*c*	*a*	*c*	*a*	*c*	*a*	*c*	*a*	*c*	*a*	*c*
0	6.72	7.95	5.92	7.28	6.93	8.225	5.56	6.93	4.99	6.525	6.01	7.45
10,000	6.88	8.06	6.05	7.35	7.22	8.405	5.76	7.05	5.16	6.60	6.32	7.57
20,000	7.19	8.18	6.2	7.48	7.72	8.675	6.06	7.2	5.32	6.705	6.83	7.96
30,000	7.67	8.77	6.4	7.64	8.5	9.295	6.7	7.4	5.54	6.795	7.88	8.82
40,000	8.43	9.97	6.62	7.84	9.51	10.755	7.77	8.28	5.85	6.925	9.16	10.64
50,000	9.37	11.4	6.9	8.06	10.66	12.765	9.22	10.02	6.33	7.105	10.68	13.13
60,000	10.54	13.73	7.27	8.3	$> t$	15.215	10.98	12.58	6.96	7.605	$> t$	16.37
70,000	11.96	16.47	7.79	8.63	/	/	$> t$	15.81	7.73	8.425	/	/
80,000	/	/	8.41	9.28	/	/	/	/	8.83	9.835	/	/
90,000	/	/	9.09	10.25	/	/	/	/	10.23	11.695	/	/
100,000	/	/	9.95	11.53	/	/	/	/	12.2	14.455	/	/
110,000	/	/	11.1	13.51	/	/	/	/	/	/	/	/
120,000	/	/	12.56	16.32	/	/	/	/	/	/	/	/

played a secondary role on decreasing the FCGR. Since the load–-displacement response shared a similar pattern with the crack growth when applying different reinforcement schemes, it might be used as an auxiliary evaluation criterion towards the CRS reinforcement on surface cracks.

This experimental study, which was conducted under laboratory conditions, intended to pave a way for the CRS repairing on surface cracked offshore metallic pipes. Its difference from the under subsea conditions is existing undoubtedly, in terms of the underwater curing and loading protocol. In such a sense, further related underwater investigations are expected to promote studies and applications of CRS in the offshore industry.

CRediT authorship contribution statement

Zongchen Li: Conceptualization, Methodology, Validation, Formal analysis, Data curation, Writing - original draft, Writing - review & editing, Visualization. **Xiaoli Jiang:** Conceptualization, Writing - review & editing, Supervision. **Hans Hopman:** Supervision, Funding acquisition. **Ling Zhu:** Resources, Funding acquisition. **Zhiping Liu:** Resources, Funding acquisition.

Declaration of Competing Interest

The authors declare that they have no known competing financial interests or personal relationships that could have appeared to

influence the work reported in this paper.

Acknowledgement

The authors appreciate Department of Maritime and Transport Technology, Delft University of Technology, the Netherlands for sponsoring this research. The experimental investigation was supported by Overseas Expertise Introduction Project for Discipline Innovation – 111 project of Chinese Ministry of Education and State Administration of Foreign Experts Affair of P. R. China [grant number 444110356] and Department of Maritime and Transport Technology, Delft University of Technology, the Netherlands. The Key Laboratory of High Performance Ship Structure of the Chinese Ministry of Education is also appreciated for providing the experimental facilities. The first author would like to acknowledge the China Scholarship Council, P. R. China [grant number 201606950024] for funding his research.

Appendix. –Test results of the surface crack growth in steel pipes

(See Table A1)

References

[1] Z. Li, X. Jiang, H. Hopman, Engineering, “Surface Crack Growth in Offshore Metallic Pipes under Cyclic Loads: A Literature Review”, Journal of Marine Science and Engineering 8 (2020) 339.
[2] Z. Li, X. Jiang, H. Hopman, L. Zhu, Z. Liu, An investigation on the circumferential surface crack growth in steel pipes subjected to fatigue bending, Theor. Appl. Fract. Mech. 105 (2020) 102403.
[3] DNV, DNV-RP-F108: Assessment of flaws in pipeline and riser girth welds, 2017.
[4] A. P. I. API, 579-1/ASME FFS-1: Fitness-for-service, 2016.
[5] N. Saeed, H. Ronagh, A. Virk, Composite repair of pipelines, considering the effect of live pressure-analytical and numerical models with respect to ISO/TS 24817 and ASME PCC-2, Compos. B Eng. 58 (2014) 605–610.
[6] T. Tafsirojjaman, S. Fawzia, D. Thambiratnam, X.-L. Zhao, Behaviour of CFRP strengthened CHS members under monotonic and cyclic loading, Compos. Struct. 220 (2019) 592–601.
[7] Z. Li, X. Jiang, and G. Lodewijks, The latest development of reinforcement techniques on tubular joints, in: Progress in the Analysis and Design of Marine Structures, pp. 783-790, 2017.
[8] BS, BS EN ISO 24817:2015. Petroleum, petrochemical and natural gas industries-Composite repairs for pipework-Qualification and design, installation, testing and inspection: British Standards Institution, 2015.
[9] ASME, ASME PCC-2: Repair of Pressure Equipment and Piping: American Society of Mechanical Engineers, 2015.
[10] K.S. Woo, J.S. Ahn, S.H. Yang, Cylindrical discrete-layer model for analysis of circumferential cracked pipes with externally bonded composite materials, Compos. Struct. 143 (2016) 317–323.
[11] H. Zarrinzadeh, M. Kabir, A. Deylami, Experimental and numerical fatigue crack growth of an aluminium pipe repaired by composite patch, Eng. Struct. 133 (2017) 24–32.
[12] A. Achour, A. Albedah, F. Benyahia, B.A.B. Bouiadjra, D. Ouinas, Analysis of repaired cracks with bonded composite wrap in pipes under bending, J. Pressure Vessel Technol. 138 (2016) 060909.
[13] Z. Valadi, H. Bayesteh, S. Mohammadi, XFEM fracture analysis of cracked pipeline with and without FRP composite repairs, Mechanics of Advanced Materials Structures (2018) 1–12.
[14] A.A. Abd-Elhady, H.E.-D.M. Sallam, I.M. Alarifi, R.A. Malik, T.M. El-Bagory, Investigation of fatigue crack propagation in steel pipeline repaired by glass fiber reinforced polymer, Compos. Struct. 242 (2020) 112189.
[15] H. Zarrinzadeh, M. Kabir, A. Deylami, Crack growth and debonding analysis of an aluminum pipe repaired by composite patch under fatigue loading, Thin-Walled Structures 112 (2017) 140–148.
[16] B. Zheng, M. Dawood, Fatigue crack growth analysis of steel elements reinforced with shape memory alloy (SMA)/fiber reinforced polymer (FRP) composite patches, Compos. Struct. 164 (2017) 158–169.
[17] J. Chen, H. Pan, Stress intensity factor of semi-elliptical surface crack in a cylinder with hoop wrapped composite layer, Int. J. Press. Vessels Pip. 110 (2013) 77–81.
[18] Z. Li, X. Jiang, H. Hopman, Ships and offshore structures (2019) 1.
[19] Z. Li, X. Jiang, H. Hopman, L. Zhu, Z. Liu, W. Tang, Mechanics of Advanced Materials Structures (2020) 1–15.
[20] Z. Li, X. Jiang, H. Hopman, L. Zhu, Z. Liu, Numerical investigation on the surface crack growth in FRP-reinforced steel plates subjected to tension, Theor. Appl. Fract. Mech. (2020) 102659.
[21] API, API SPEC 5L:Specification for Line Pipe, ed. Washington, D.C.: American Petroleum Institute, 2018.
[22] ASTM, ASTM E2899. Standard Test Method for Measurement of Initiation Toughness in Surface Cracks Under Tension and Bending. West Conshohocken, United States: ASTM, 2019.
[23] ASTM, ASTM E647. Standard Test Method for Measurement of Fatigue Crack Growth Rates, 1994.
[24] S. Kim, M.-H. Kim, Dynamic behaviors of conventional SCR and lazy-wave SCR for FPSOs in deepwater, Ocean Eng. 106 (2015) 396–414.
[25] M. Kabir, S. Fawzia, T. Chan, J. Gamage, J. Bai, Experimental and numerical investigation of the behaviour of CFRP strengthened CHS beams subjected to bending, Eng. Struct. 113 (2016) 160–173.